3 Airborne Measurement Technologies

3-1 Airborne Multiparameter Precipitation Radar (CAMPR) Observation of Wind Fields in Snow Clouds

SATOH Shinsuke, HANADO Hiroshi, NAKAGAWA Katsuhiro, IGUCHI Toshio, NAKAMURA Kenji, and YOSHIZAKI Masanori

The CRL airborne multiparameter precipitation radar (CAMPR-D) is equipped with a dual-beam antenna to measure three-dimensional wind fields in precipitation. This paper describes the methods and related problems of wind-vector calculation, and shows the results of dual-Doppler analysis. The observation data was obtained through the WMO-01 (Winter MCSs Observations over the Japan Sea 2001), the objective of which was to reveal the structure of snow clouds over the Japan Sea. First, the trajectories of the front- and rear-antenna beam were investigated. The results showed that there were some gaps between the two beam footprints due to the speed and direction of the wind relative to the aircraft, and that the front beam did not overlap the rear beam in some regions on the leeward side. The investigation also demonstrated that the data from a flight-information system (POS) consisting of an optical-fiber gyroscope and a differential GPS is effective in removing the aircraft velocity component from the measured Doppler velocity. Finally, some distributions of the wind vectors in the along-track vertical sections are shown. The wind vectors were analyzed using the observation data for linear clouds in the JPCZ (Japan Sea Polar-airmass Convergence Zone). The distributions showed that updrafts were dominant over the sea because of developing convective cells, and that the repetition of updrafts and downdrafts seemed to indicate roll convections. The distributions also showed a common structure of anvil echoes that extended northward or northeastward.

Keywords
Airborne radar, Dual-Doppler, Wind field, Snow cloud

1 Introduction

Between 1990 and 1995, the Communications Research Laboratory developed a CRL Airborne Multiparameter Precipitation Radar (or "CAMPR")[1]. This radar was invented to develop measurement technology for the precipitation radar (PR) installed in the Tropical Rainfall Measuring Mission (TRMM) satellite [2]. The CAMPR was used for ground validation of the TRMM after its launch[3]. In addition to the TRMM validation experiments, we performed measurements of mesoscale convective systems using the CAMPR, collaborating with a number of research institutes[4]~[7]. Further, in 1996 and 1997, we developed an antenna unit having a dual-Doppler function and a dual-polarization coherent transceiver function, separate from the previous slot-array antenna, and carried out a number of observation flights[8][9]. For convenience, we will refer to the radar equipped with the

first slot-array antenna as "CAMPR-A" and that equipped with the dual-beam antenna as "CAMPR-D." The CAMPR-A has a relatively sharp antenna beam, but it has the disadvantage of poor coherency between the horizontal and vertical polarization antennas. Therefore we have employed the CAMPR-D in observation flights since 1997. Also, another system using an offset parabolic antenna for ground observation, referred to as "CAMPR-G," is used for ground observation[10]; i.e., for purposes other than those involved in aircraft observation.

There are a few examples of the application of airborne dual-Doppler radar in the United States, whereas the CAMPR-D is the only example of this type of radar in Japan. For example, the ELDORA (Electra Doppler Radar)[11][12], of the National Center for Atmospheric Research (NCAR), can perform dual-Doppler measurement in all directions through 360-degree rotation of two slot antennas installed in a radome in the tail of a medium-sized propeller plane (Electra). This X-band (10-GHz) radar can measure the three-dimensional wind field and the three-dimensional precipitation distribution, while conducting in situ observation of cloud physics by in-cloud flight at a relatively low altitude. A substantially similar radar is installed in the P-3 aircraft of the National Oceanic and Atmospheric Administration (NOAA) and has been used in diverse field experiments, along with Electra. Another example of such a radar is the EDOP (ER-2 Doppler Radar), installed in a small jet plane (ER-2) of the National Aeronautics and Space Administration (NASA). This radar can conduct dual-Doppler measurements using two small offset parabolic antennas[13][14]. The ER-2 flies at high speeds and at high altitudes (about 20 km), and its antennas are fixed in the nadir and forward directions. On the other hand, the CAMPR-D, carried in a small propeller plane (Beachcraft B-200), can perform dual-Doppler measurements using two small lens-horn antennas housed in a radome in the bottom of the aircraft. The B-200's limitations are that the maximum flight altitude is about nine kilometers and the cruise duration is about three hours. However, it can take off and land at a small airport, allowing for speedy, agile measurement operations. In this way, the airborne dual-Doppler radars are designed to suit the characteristics of the mother aircraft, with individual advantages and disadvantages. Despite these differences, these radars share the same basic approach to determining the three-dimensional wind distribution in a target area of precipitation. Namely, they generate a front beam and a rear/nadir beam with two antennas, and the Doppler velocity vectors for two directions are synthesized on the assumption that wind is steady during the period of time required for the two radar beams to overlap. Since the duration is several minutes at most, the measurement may be more precisely termed a quasi dual-Doppler measurement. In the case of the ELDORA, a number of examples of three-dimensional wind field analyses have been reported, and the analysis technique using the dual-Doppler radar has been almost completely established. On the other hand, in the case of the CAMPR-D, which represents an entirely different radar system, there have been no examples of calculation of an actual wind-velocity distribution.

This paper describes the method of analyzing the three-dimensional structure of the mesoscale precipitation—particularly the wind field—together with a discussion of related issues, focusing on the dual-Doppler function of the CAMPR-D. The observation data used in the present analysis was taken in the course of a comprehensive field experiment—the WMO-01 (Winter Mesoscale Convective Systems Observations over the Japan Sea-2001)[9]. The purpose of using CAMPR-D in the WMO-01 includes the clarification of the structure and mechanism of snow clouds offshore over the Japan Sea, which have been subject to almost no investigation, and the observations of snow clouds over mountains, which are difficult to conduct with ground-based radar. Another aim is to collect data related to the microphysics of snow clouds,

required for the development and design of a next-generation satellite-borne dual-frequency radar. In addition, we conducted simultaneous measurement using another airplane (Gulf Stream II)—performing in situ observation of cloud and snow particles—along with an airborne cloud profiling radar (SPIDER). We also carried out flight observation over an area covered by the ground-based Doppler radar network, in order to validate the wind vectors provided by the CAMPR-D. What is particularly interesting in terms of meteorology is the structure of convective clouds formed in the JPCZ (Japan Sea Polar-airmass Convergence Zone), which shows significant convection and brings heavy snowfall on the coastal areas along the Japan Sea. Specifically, it is important to investigate the three-dimensional airflow structure of the convective clouds over the sea using the CAMPR-D data, with its high resolution in the vertical direction. The goal of this research is to establish a technique for analyzing Doppler velocity data and to clarify the problems we must bear in mind when calculating wind fields.

2 Structure of CAMPR-D

Fig.1 shows the schematic structure and a photo of the antenna unit of the CAMPR-D. To realize the dual-Doppler function, two lens-horn antennas and reflection mirrors are coupled to form two beams aimed in different directions. The two antennas and mirrors are rotated by a motor to conduct an antenna scan over the −60 to +85-degree range in the roll direction (the nadir direction is set at zero degree). The scan speed is variable from 1-17 degrees per second, and step scanning is possible at desired angular intervals. The reflection mirrors are installed to tilt the front antenna beam forward by +31 degrees along the heading direction of the aircraft and the rear antenna beam backward by −4 degrees relative to the nadir direction. The two antenna beams therefore feature an angle differential of 35 degrees. This value has been determined in accordance both with the request for

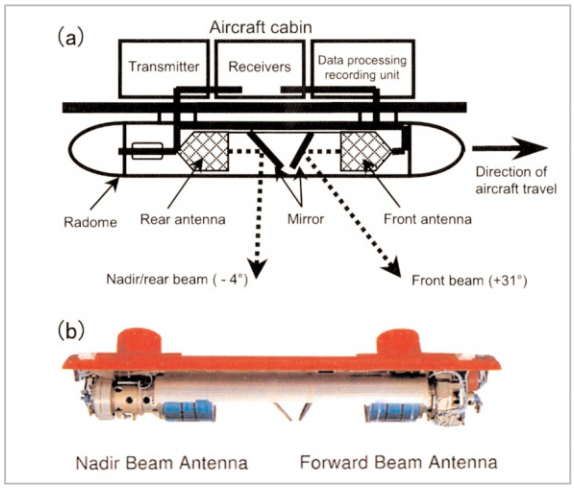

Fig.1 *(a) Schematic diagram of the structure of CAMPR-D and the antenna unit*
(b) Photo of the antenna unit without radome

improved accuracy in synthesizing the two Doppler velocity vectors and with the contradictory request for a shorter time span between observations made by the two beams. In the case of the airborne dual-Doppler radar in the US, the angular difference between the two beams is also 30-35 degrees. In the case of the CAMPR-D, the angle of the rear beam was determined so as to directly measure the vertical velocity of falling precipitation particles (the sum of the terminal falling velocity and the vertical velocity) at an antenna-scanning angle of zero degree. The angle of −4 degrees was determined with reference to the offset of the average pitch angle (+1-3 degrees) during previous observation flights and the pitch reference angle. Please refer to additional materials[1][4][5] with respect to the radar specifications for units other than the antenna.

3 Method of flight observation

Fig.2 presents a schematic view of dual-Doppler observation using the dual-beam antenna. In principle, the plane (B-200) flies straight and performs scanning with both the front and rear beam antennas at the same time. The front antenna and the rear antenna are alternately switched to transmit signals at two

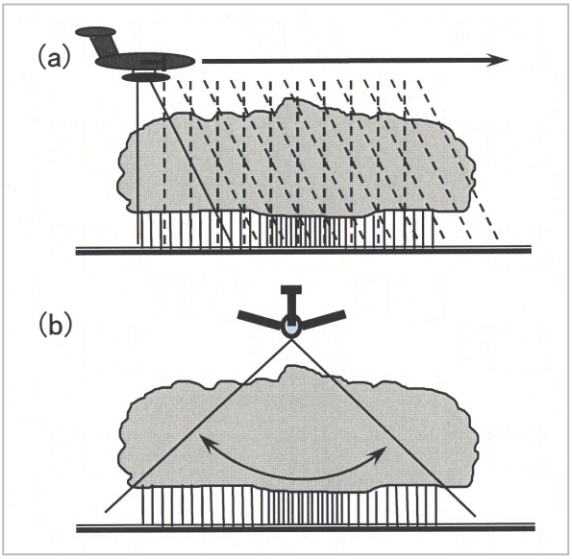

Fig.2 *Schematic description of the dual-Doppler observation using the CAMPR-dual beam antennas*
(a) Right-side view along the direction of travel
(b) Rear view

pulse intervals (in most cases). The reason for switching every two pulses is to shorten the pulse-repetition intervals when calculating the Doppler velocity based on the pulse-pair method. Since the relative cruising speed of the aircraft relative to ground may double or even triple due to the effect of winds, the antenna scan is performed over a large range (for example, $\pm$60 degrees) in the event of oncoming winds and over a small range (for example, $\pm$35 degrees) in the event of tail-winds. Since the cruising speed of the aircraft relative to the ground is around 80-140 m/s and its flight altitude is usually 6-8 km, the required time for the two beams to reach the same spot is shorter than about 70 seconds ($8{,}000 \times \tan 35°/80$) if the spot is located inside the vertical cross-section (Fig.2a) beneath the aircraft. Even when the antenna-scanning angle is large, the effective measurement range is about 20 km. Since this time difference is shorter than three minutes, changes over time in precipitation echo and wind fields are expected to be negligible in most cases.

Fig.3 shows all of the CAMPR-D observation-flight legs, flown twelve times between January 6 and January 30 during the WMO-01 (Winter MCSs Observations over the Japan Sea-2001). The plane in question flew from Nagoya Airport through January 27, and flew from Niigata Airport thereafter. The observation flights far offshore over the Japan Sea were limited by the cruising duration of the aircraft (three hours or less) and flight regulations on weekdays in the training zone of the Self Defense Forces. The trajectories of the dual beams transmitted from the two antennas have been investigated with reference to the actual flight data. Fig.4 shows a portion of the trajectory of the second observation flight, made on January 14. The airplane at first flew to the west-northwest, then went to the northeast, performing a $\pm$60° scan; it then headed southeast to perform a $\pm$35° scan, and finally flew to the southwest with a $\pm$60° scan. During this flight, the altitude of the aircraft was about seven kilometers, and the wind at this altitude blew nearly westerly at high speeds (nearly 50 m/s). If a $\pm$60° scan is performed in tailwinds, as in the case of the flight leg to the northeast, gaps appear between the footprints during the continuous scan. Therefore, the scan should be conducted at shorter intervals. A greater problem is that the path of the aircraft nose differs from the actual traveling direction (i.e., there is a large drift angle) when the aircraft is exposed to strong side winds. Under such conditions, the target echo may not be captured by both beams, because the front beam has moved apart from the rear beam. In the example shown in Fig.4, the drift angle was particularly large in the legs to the northeast and to the southwest, and the trajectories of the front beam (which provided the conical scan) were bent on the downstream side. When the aircraft flies parallel to the wind, such problems do not occur. When the aircraft is chasing clouds to conduct observations in precipitation areas, however, it sometimes has to fly in the direction perpendicular to the wind. In this case, since the aircraft will fly tilting its nose into the oncoming wind, we must take into consideration the possibility that dual-Doppler observation will not be possible in a portion of the leeward areas if the

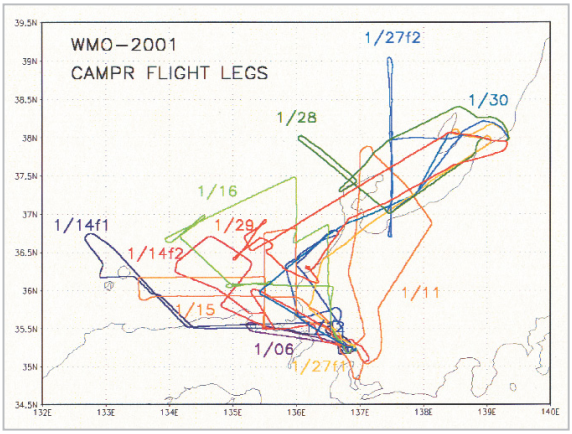

Fig.3 *Flight courses of 12 CAMPR field experiments during the WMO-01 observation period*

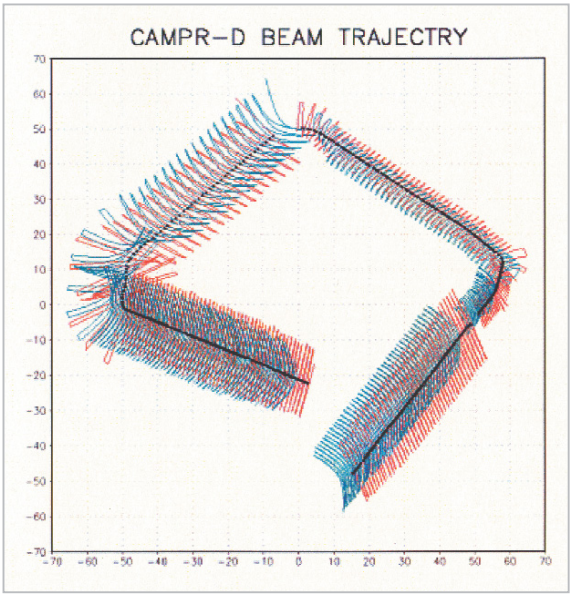

Fig.4 *Trajectories of the center of the front beam (blue) and the nadir/rear antenna beam (red) in the horizontal cross-section at an altitude of 1 km The black points represent the position of the aircraft when the antenna is directed in the nadir direction. The aircraft flew clockwise, and this example shows a portion of the data for the second flight on January 14, 2001.*

winds are too strong.

There are a number of observation methods other than the above-described basic flight modes for dual-Doppler observation. For example, if the convective cloud is so high that the B200 cannot fly over the top, it may conduct only a left-side scan, flying along the cloud wall to view the cloud from the left. If the area of precipitation is large, the aircraft may continue to fly in a straight line for a long period. In contrast, if the target cloud is small, the aircraft may fly around it or fly in the shape of a cross within the cloud. If the aircraft makes more than one round trip in the same flight or if echo continues along the flight course, the antenna may be fixed in the nadir direction, with only the rear antenna available for dual-polarization transmission, and observation may be conducted using the IQ mode, which records all pulse bits of the two receivers. When the flight altitude changes during lift-off and landing, the antenna may be fixed in a nearly horizontal direction (+85°) for dual polarization measurement.

4 Analysis of Doppler data

The analysis of the Doppler data taken by the CAMPR-D system consists of three steps: (1) removal of the aircraft velocity component included in the Doppler velocity and correction of the Doppler velocity folding, (2) conversion of the measurement data into the three-dimensional Cartesian coordinates, and (3) synthesis of the Doppler velocity elements of the front and rear beams. Fig.5 illustrates the coordinate system for the aircraft used in this analysis. It is important to handle all the data in the right-hand coordinate system, assuming that the direction of the plane nose is the X-axis (i.e., the heading direction). In this section we will omit a detailed descriptions of equations and instead explain the

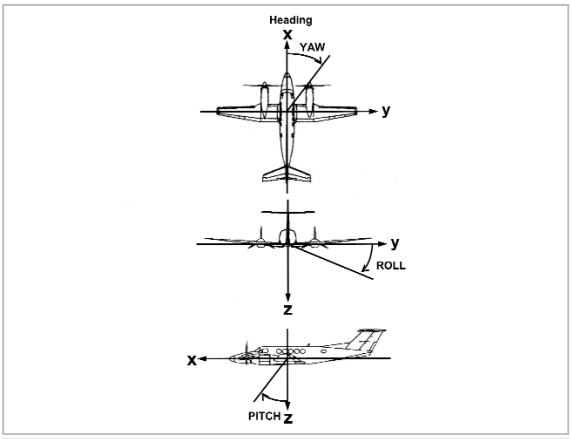

Fig.5 *A standard coordinate using a reference point of the aircraft for the POS and velocity data analysis*

problems accompanying the respective procedures.

In order to remove the aircraft velocity component included in the Doppler velocity data, we have to know the aircraft's speed relative to the ground. If the three components of the aircraft's relative speed are identified, it is easy to calculate the velocity component in the direction of the antenna beam. In 1998 and earlier, however, flight information data for B200's attitude, position, and speed was limited to that acquired at intervals of one second by a system (the "FDS") composed of a mechanical gyroscope, a pressure altimeter, and a GPS signal receiver. In particular, the poor accuracy regarding the aircraft's speed relative to the ground (calculated based on the GPS position and time data) posed a significant problem. In contrast, the new flight information system used in this study (referred to as the "POS"), composed of an optical-fiber gyroscope and a differential-GPS (DGPS) receiver, provides the north, east, and downward velocity components, as well as latitude, longitude, and altitude data of the plane (obtained by two-way analysis) at 50 Hz (at intervals of 0.02 seconds). In addition, roll, pitch, heading, and yaw angles are measured with high precision using the system. Using this POS data, the CAMPR system time (provided every 0.01 seconds) was corrected by the GPS time. The system time correction made it possible to correct the Doppler velocity components of the aircraft every integration pulse time [for example, every 0.064 seconds at a pulse-repetition frequency (PRF) of 4 kHz with an integration pulse number of 256]. Since the speed of the aircraft may reach 130 m/s or more with a tailwind, however, we must pay attention to error in the pitch angle. For example, if the pitch angle increases by one degree, large aircraft velocity components are introduced: 2.3 m/s in the nadir beam and 76.4 m/s in the front beam tilted 35 degrees. This means that even a slight error in the pitch angle affects the measured Doppler velocity, which is otherwise performed with an accuracy of 0.1 m/s or higher. On the other hand, since this error is common to all data, it can be removed as an offset by a correction that renders the speed at the ground level statistically zero. In the current analysis, we ensured that the velocity was almost zero relative to the ground for specified data. However, an issue remained in that the ground speed was not zero for all beams affected by problems related to sidelobe effects and ground-surface conditions. In addition, the apparent Doppler velocity measured with the aircraft speed component included may contain double or triple foldings, particularly in the front beam. In such cases it is extremely difficult to imagine the true Doppler velocity. However, the correction of such folding effects in calculating Doppler velocity becomes relatively easy if the component of aircraft speed is removed using the method described above. Another problem that must be addressed is the difficulty in correcting the folding effect using a simple algorithm that assumes no folding on the ground surface beneath the aircraft and that corrects the folding effect based on a continuity of velocity from this ground point. In this study, we have adopted another algorithm to correct the folding velocity using a reference of vertical wind velocity profiles, measured with a rawin-sonde and other means.

The method of converting the measured data into a three-dimensional grid (x, y, z) is expressed by:

$$x = r \sin(P)$$
$$y = r \cos(P) \sin(R)$$
$$z = r \cos(P) \cos(R),$$

where r is the distance in the range direction, P is the pitch angle plus the antenna mounting angle, and R is the roll angle plus the antenna scan angle. In principle, the synthesis of Doppler velocities in two directions in the three-dimensional grid is equal to the dual-Doppler synthesis attained using ground radar. However, if the scan angle is small (less than approximately ± 15 degrees), the portion of the horizontal wind component included in the measured Doppler velocity is small, and therefore it is difficult to calculate the cross-tracking horizontal wind vector, which is perpendi-

cular to the heading direction. The vertical and horizontal wind vectors along the heading direction can be calculated with rather high accuracy, setting aside problems relating to the separation of the terminal falling velocity of the precipitation particles. If the cross-tracking wind vectors are calculated from the velocity data obtained at large scanning angles, it is also relatively easy to derive the vertical profile of the real horizontal wind vectors by coupling them with the along-tracking horizontal wind vectors. Calculation of the three-dimensional wind vectors requires the use of the mass-continuity equation for the air. In order to solve this equation, we have to apply the variational method under boundary conditions stipulating that the vertical wind velocity is zero on the ground and at the top of the cloud, with appropriate weighting of the horizontal and vertical wind components, depending on the antenna angles. In this paper, we have calculated the wind vector in the vertical cross-section in the heading direction of the aircraft to enable easy synthesis of velocity vectors. Using the data obtained at R = 0, the horizontal wind component in the heading direction, U, and the vertical wind component, W (positive when directed downward), are expressed by the following equations:

$$U = \{V_F \cos(P_H) - V_H \cos(P_F)\} / \sin(P_F - P_H)$$

$$W = \{V_H \sin(P_F) - V_F \sin(P_H)\} / \sin(P_F - P_H) - Wt$$

where V is the observed Doppler velocity and the subscripts F and H represent the front beam and rear beam, respectively. Wt is the terminal falling velocity of the precipitation particles, expressed as a function of the reflectivity Z. In this study, we have adopted the following empirical equation for snowflakes:

$$Wt = 0.75 \times Z^{0.0714}$$

5 Results

Fig.6 shows an infrared image taken with the meteorological satellite Himawari at 13:00 JST on January 16, when the present analysis

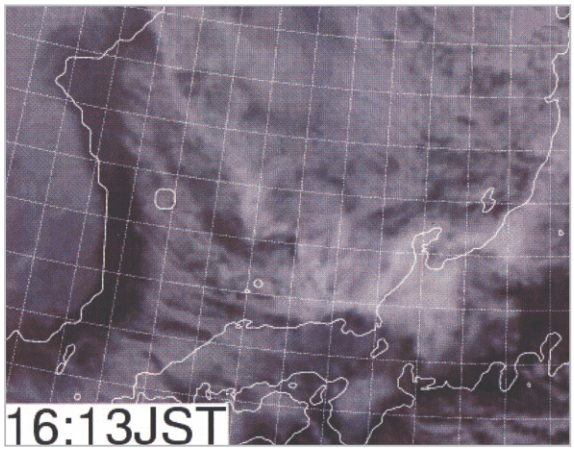

Fig.6 *Infrared image taken by the meteorological satellite Himawari at 13:00 JST on January 16, 2001*

was made. The developed cloud-band extending from the continent to the southeast is the Japan Sea Polar-airmass Convergence Zone (JPCZ). On the northeast side of the JPCZ, some traverse-mode linear clouds (T-mode clouds), which are almost perpendicular to the monsoon wind direction, are seen. A vortex disturbance is identified off the coast of Sanin, and on its southern side it merges with the longitudinal-mode linear cloud (L-mode cloud) extending from the west, forming a significant snow cloud in Wakasa Bay. Fig.7 presents the combination of the three CAMPR flight legs (LEG A, LEG B, and LEG C) for analysis, as well as the observation time, superimposed on a composite ground-based radar map provided by the Japan Meteorological Agency. In LEG A, the data collected indicated the likely occurrence of an echo caused by either a T-mode cloud that was merging with the JPCZ or a spiral band comprising the vortex disturbance. Figs.8, 9, and 10 each show the echo intensity distribution, horizontal wind vector, and vertical wind vector inside the vertical cross-section along the respective flight legs. The bottom figure shows the echo intensity distribution in the horizontal cross-section at an altitude of 1.5 km. Although the actual horizontal wind vectors in the vertical cross-section represent the components in the heading direction, we may conclude that the wind vectors shown in these diagrams indicate parallel components to the

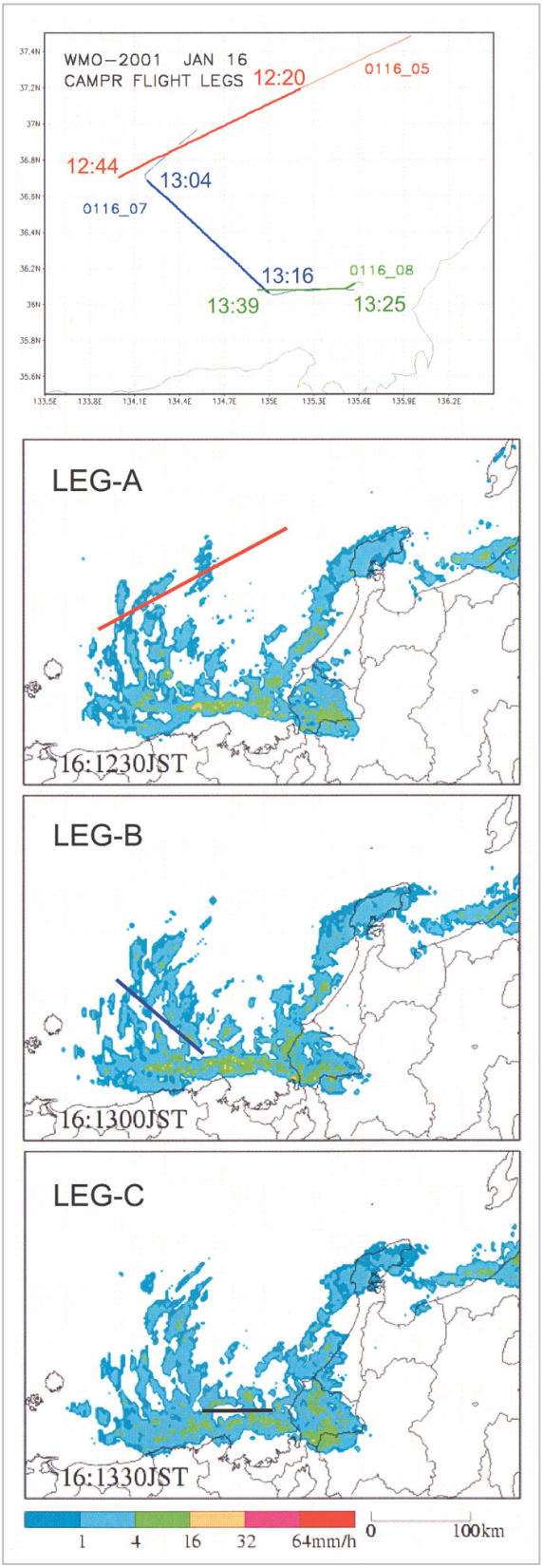

Fig.7 *Three observation-flight legs for analysis and the composite maps of the Japan Meteorological Agency's radar images for west Hokuriku at that time*

vertical cross-section, since the traveling direction of the aircraft nearly agrees with the heading direction (in most cases, the drift angle is less than 10 degrees). Fig.8 indicates that the echo on the west side extends to the northeast as the altitude grows, and that the wind vector indicates an updraft to the northeast. These sorts of anvil echoes extending to the northeast are often seen among other data—in the cross-track direction in LEG B, for example (figure not shown)—and seem to be a common feature in the snow clouds near the JPCZ observed in our experiment. The horizontal cross-section at an altitude of 1.5 km indicates that these two echoes are independent clusters, which have a size of 20-30 km. Next, the vertical cross-section along LEG B is the result of an observation made along the JPCZ. The horizontal cross-section shows a continuous echo on the southeast side 50 km away in the horizontal direction (Fig.9). Although the vertical cross-section shows an echo tilted to the northwest on the upstream side, the air-flow structure is expressed by vectors directed upward to the southeast. However, considering the relative flow in the convective cell, a lower wind velocity in the upper layer relative to that of the lower layer indicates that the relative wind vector is directed to the northwest in the upper layer. This interpretation is consistent with the tilt of the echo. This echo is the most developed one, and its echo top height is about 4.5 km. Another feature is that updraft areas and downdraft areas appear alternately at 5-10 km intervals in lower layers below an altitude of three kilometers on the southeast side, where continuous echoes are observed. This may represent convective-cell circulation inside a band-like echo, probably indicating a cross-section of a roll convection. LEG C, shown in Fig.10, consisted of a flight close to the northern side of the strong band echo extending in the east-west direction. On the northern side of the strong echo (seen at a horizontal distance of 30-40 km in the horizontal cross-section at an altitude of 1.5 km), the cross-section shows that the echo does not reach the ground,

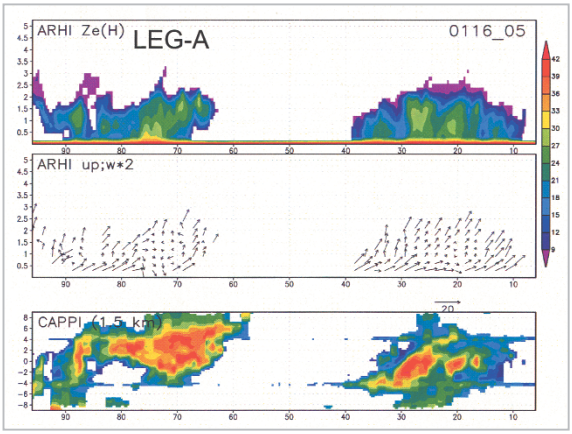

Fig.8 *Radar reflectivity (top) in the vertical cross-section along LEG A; wind vectors (middle); and reflectivity in the horizontal cross-section at an altitude of 1.5 km (bottom)*

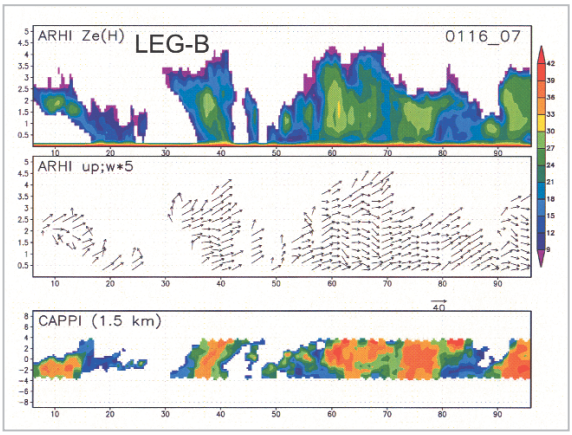

Fig.9 *Same as Fig.8 in the cross-section along LEG B*

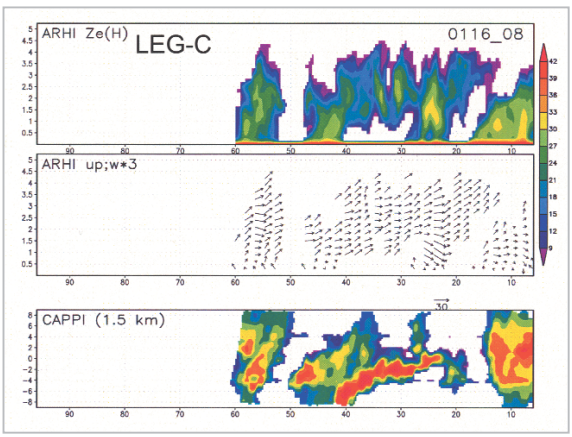

Fig.10 *Same as Fig. 8 in the cross-section along LEG C*

and that it represents an anvil echo extending from the south convective cell to the north. Considering the strong updrafts in the figure, we can conclude that this is a significantly tilted echo under development, rather than an anvil echo with a flow of snow particles. It appears that an echo, which extended eastward from a point located 15 km in the horizontal direction, was affected by land and therefore featured a gentle distribution with a low echo-top height.

6 Summary and future plans

This paper has explained the dual-Doppler function of the CAMPR-D and the basic data-analysis methods, along with a discussion of related problems. We first described the mechanical structure of the dual-beam antenna and then showed the trajectories of the front and rear beams using actual observation-flight data. Since the cruising speed of the aircraft varies significantly depending on its motion relative to the wind, we must control the antenna-scanning range so as to leave no gap between the beam footprints. Also, we must take into consideration that there will be regions on the leeward side where the front beam does not overlap the rear beam due to drift angles in the event that the aircraft is exposed to strong side winds during flight. We have indicated that the aircraft velocity component can be removed from the measured Doppler velocity data by utilizing the POS data provided by an optical-fiber gyroscope and the DGPS. This was not attainable using a conventional mechanical gyroscope and the GPS alone. This technique is therefore expected to be able to improve the analysis of Doppler data in the future. However, a slight error in the measured pitch angle may introduce a large aircraft-speed component error in the observed Doppler velocity. Therefore we must improve pitch-angle measurement accuracy through the use of statistics relating to Doppler velocities on the ground surface. Moreover, since the antenna beam width of the CAMPR-D is very large (about seven degrees), some errors in echo intensity and Doppler velocity due to non-uniform beam filing will represent serious problems, which should be investigated in more detail.

Most of the wind vectors in the vertical cross-section derived in the current analysis tended to be updrafts in many regions. This is probably because echoes under development are dominant over the Japan Sea. In the present analysis, we employed the Z-Wt equation for snowflakes when calculating the falling velocity of precipitation particles. Since the strong-reflectivity echoes probably originate from graupels, their true falling velocity is greater, and therefore the analyzed vertical wind velocity should be much greater. In terms of the structure of convective clouds along the JPCZ, analysis has not reached a level permitting the construction of a conceptual model. The convective echoes over the sea share common characteristics in that anvil echoes that accompany tilted updrafts are significantly observed and in that most of them are directed to the northeast and to the north—namely, in the direction of extension of the T-mode echo. In addition, alternating updrafts and downdrafts (probably indicating the existence of roll convections) were observed at 5-10 km intervals in the vertical cross-section along the JPCZ. We intend to clarify the structure of convective clouds in the JPCZ, accumulating case studies that will take into account the evolution of individual convective cells that form the respective echoes.

The present analysis investigated only the structure of air-flow in the vertical cross-section along each flight leg. However, it is also possible to calculate the wind vectors in the vertical cross-section along the cross-track direction (direction of antenna scanning) as well as wind vectors in three-dimensional space, if the mass-continuity equation is employed. Such calculations, however, require a technique for integrating the equation using weighted Doppler velocities and the variational method. This is one of the challenges we will face in the future.

Acknowledgments

We are grateful to the Nakanihon Air Service Co., Ltd. for their cooperation in flight services for the field experiments and in POS data collection and processing. We also would like to thank the observation members of the WMO-01 for their help with the flight experiments. This experiment was supported by the Japan Science and Technology Corporation, as part of the project “Studies on Structure and Formation/Development Mechanisms of Mesoscale Convective Systems” of the Core Research for Evolutional Science and Technology.

References

1 H. Kumagai, K. Nakamura, H. Hanado, K. Okamoto, N. Hosaka, N. Miyano, T. Kozu, N. Takahashi, T. Iguchi, and H. Miyauchi, "CRL airborne multiparameter precipitation radar (CAMPR): System description and preliminary results", IEICE Trans. Com., E79-B, No.6, pp. 770-778, 1996.

2 S. Satoh, "Achievements of airborne/spaceborne precipitation radar observation techniques", Joho-Tsushin Journal, Vol.16, No.3, pp. 19-21. 1998 (in Japanese).

3 R. Oki, K. Furukawa, S. Shimizu, Y. Suzuki, S. Satoh, H. Hanado, K. Okamoto, and K. Nakamura, "Preliminary results of TRMM: Part 1, A comparison of PR with ground observations", Marine Tech. Soc. J., Vol. 32, No.4, pp. 13-23, 1999.

4 N. Takahashi, H. Kumagai, H. Hanado, T. Kozu, and K. Okamoto, "The CRL airborne multiparameter precipitation radar (CAMPR) and the first observation results", Proc. 27th Conf. on Radar Meteor., Vail, pp. 83-85, 1995.

5 N. Takahashi, H. Hanado, and S. Satoh, "Measurement of kinematics and precipitations of stratiform rainfall with airborne multiparameter rain radar", Proc. 12th Int. Conf. on Cloud and Precip., Zurich, Switzerland, pp. 450-453, 1996.

6 S. Satoh, T. Iguchi, H. Hanado, N. Takahashi, H. Horie, H. Kumagai, and T. Kozu, "Airborne multiparameter radar observation of Baiu-frontal precipitation during TREX in 1996", Proc. 28th Conf. on Radar Meteor., Austin, TX, pp. 71-72, 1997.

7 TREX observation group, "A report on TREX (Torrential Rainfall Experiment)", Tenki, Vol.45, No.2, pp.137-144, 1998 (in Japanese).

8 M. Yoshizaki, H. Seko, T. Kato, Y. Shoji, H. Eito, K. Bessho, H. Goda, and X-BAIU-99 observation group, "A report on a special observation of Baiu over East China Sea and Kyushu in 1999 (X-BAIU-99)", Tenki, Vol.47, No.3, pp.217-224, 2000 (in Japanese).

9 M. Yoshizaki, T. Kato, H. Eito, A. Adachi, M. Murakami, S. Hayashi, and WMO-01 observation group, "A report on Winter MCSs (mesoscale convective systems) Observation over the Japan Sea in January 2001 (WMO-01)", Tenki, Vol.48, No.12, pp.893-903, 2001 (in Japanese).

10 K. I. Timothy, T. Iguchi, Y. Ohsaki, H. Horie, H. Hanado, and H. Kumagai, "Test of the specific differential propagation phase shift (KDP) technique for rain-rate estimation with a Ku-band rain radar", J. Atmos. Ocean. Tech., Vol. 16, pp. 1077-1091, 1999.

11 P. H. Hildebrand, C. A. Walther, C. Frush, J. Testud, and F. Baudin, "The ELDORA/ASTRAIA airborne Doppler weather radar: Goals, design, and first field tests", Porc. IEEE, Vol. 82, pp. 1873-1890, 1994.

12 P. H. Hildebrand, W.-C. Lee, C. A. Walther, C. Frush, M. Randall, E. Loew, R. Neitzel, R. Parsons, J. Testud, F. Baudin, and A. LeCornec, "The ELDORA/ASTRAIA airborne Doppler weather radar: High-resolution observations from TOGA COARE", Bull. of the Amer. Meteor. Soc., Vol. 77, No. 2, pp. 213-232, 1996.

13 G. M. Heymsfield, S. W. Bidwell, I. J. Caylor, S. Ameen, S. Nicholson, W. Boncyk, L. Miller, D. Vandemark, P. E. Racette, and L. R. Dod, "The EDOP radar system on the high-altitude NASA ER-2 aircraft", J. Atmos. Ocean. Tech., Vol. 13, pp. 795-809, 1996.

14 G. M. Heymsfield, J. B. Halverson, and I. J. Caylor, "A wintertime Gulf coast squall line observed by EDOP airborne Doppler radar", Mon. Wea. Rev. Vol. 127, pp. 2928-2950, 1999.

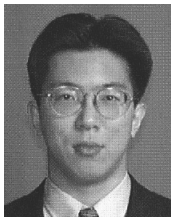

***SATOH Shinsuke**, Dr. Sci.*

Senior Researcher, Precipitation Radar Group, Applied Research and Standards Division

Radar Meteorology

***NAKAGAWA Katsuhiro**, Dr. Eng.*

Researcher, Subtropical Environment Group, Applied Research and Standards Division

Radar Hydrology

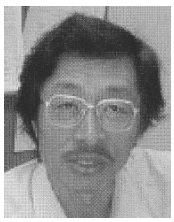

***NAKAMURA Kenji**, Ph. D.*

Director, Professor, Hydrospheric Atmospheric Research Center, Nagoya University

Radar Meteorology

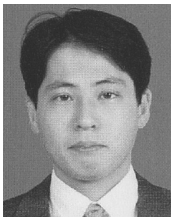

HANADO Hiroshi

Senior Researcher, Precipitation Radar Group, Applied Research and Standards Division

Microwave Remote Sensing

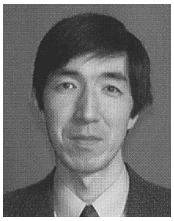

***IGUCHI Toshio**, Ph. D.*

Leader, Precipitation Radar Group, Applied Research and Standards Division

Electromagnetic Remote Sensing

***YOSHIZAKI Masanori**, Ph. D.*

Head, Forecast Research Department, Meteorological Research Institute

Mesoscale Meteorology